# Soil Freezing and Soil Water Retention Characteristics: Connection and Solute Effects

Tiantian Ma, Ph.D.[1]; Changfu Wei[2]; Xiaolong Xia[3]; Jiazuo Zhou, Ph.D.[4]; and Pan Chen, Ph.D.[5]

**Abstract:** The relation between the soil-water characteristic curve (SWCC) and the soil freezing characteristic curve (SFCC) is investigated based on the similarity between the freezing/thawing and drying/wetting behaviors of soils. The SWCCs of clay and silt are obtained by the pressure plate extractor and vapor pressure method, while the SFCCs are determined from the unfrozen water content measurement using the nuclear magnetic resonance (NMR) and temperature measurement. The pore water potential of the frozen soil is derived from a generalized Clapeyron equation, which addresses the effects of capillarity, sorption, and osmosis, and compared to that of unsaturated soils. Our experimental results show that at low water content the matric potential in the soil saturated with pore water and pore ice is generally different from that in the soil saturated with pore water and pore gas. A series of experiments on the soil samples saturated by NaCl solutions of different concentrations were performed to determine the osmotic potential and the water retention characteristics. Based on the principles of surface chemistry, a relationship between the adsorptive forces and the water film thickness is developed, which is capable of describing the soil water characteristic when the sorption effect is significant. Our results indicate that the freezing-point depression method should be applied with caution in determining the soil water retention characteristics of unsaturated soils at lower water content. **DOI: 10.1061/(ASCE)CF.1943-5509.0000851.** 

**Author keywords:** Soil-water characteristic curve; Soil freezing characteristic curve; Matric potential; Osmotic potential; Nuclear magnetic resonance (NMR).



## Introduction

The water retention behavior of unsaturated soils can be characterized using the soil-water characteristic curve (SWCC), or synonymously, the soil water retention curve (WRC), which defines the relationship between soil water potential and pore water content. This relationship is indispensable in modeling the hydromechanical behavior of unsaturated soils. A comprehensive review on the recent development of soil water retention theory can be found in Bachmann and van der Ploeg (2002). As an analog to the SWCC or WRC for unsaturated soils, the soil freezing characteristic curve (SFCC) describes the relationship among unfrozen water content, freezing soil temperature, and water potential (Koopmans and Miller 1966; Spaans and Baker 1996; Bittelli et al. 2003). The SFCC is essential to modeling the transport of water, heat, and solutes in frozen porous media (Stähli et al. 1999; Flerchinger et al. 2006; Watanabe and Wake 2009; Wen et al. 2012).

Because both the SFCC and the SWCC describe the water retention characteristics of soils, their connection has been extensively investigated from either experimental or theoretical aspects (Miller 1966; Koopmans and Miller 1966; Spaans and Baker 1996). Theoretically, it has been well recognized that the freezing characteristics can be related to the soil-water characteristics (Koopmans and Miller 1966; Miller 1980). Sufficient experimental evidence has also shown that the two characteristic curves indeed correspond very well to each other (Spaans and Baker 1996; Bittelli et al. 2003; Watanabe and Flury 2008).

In frozen soils, a certain amount of water remains unfrozen at subzero temperatures due to the lower energy potential (i.e., lower activity) of the pore water, which in turn depresses the water freezing point (Spaans and Baker 1996; Cannel and Gardner 1959; Miller 1980; Dash et al. 1995; Watanabe and Mizoguchi 2002; Watanabe and Wake 2009). Total pore water potential, which controls the unfrozen water content in frozen soil, includes two components: the matric potential and the osmotic potential (Drotz et al. 2009). The matric potential stems from the adsorptive and capillary effects in the soil (Flerchinger et al. 2004), and the osmotic potential depends on the solutes and their concentrations in the pore water. The effect of osmotic potential on the unfrozen water amount in frozen soils has been evaluated by Drotz et al. (2009) and Torrance and Schellekens (2006).

Traditionally, the total pore water potential for frozen soils is determined, via the Clapeyron equation, using the freezing point of the soil water that can be measured accurately (Spaans and Baker 1996; Drotz et al. 2009; Suzuki 2004), while the unfrozen water content is determined using a time domain reflectometry (TDR) or the nuclear magnetic resonance (NMR) method. As such, the SFCC

[1]State Key Laboratory of Geomechanics and Geotechnical Engineering, Institute of Rock and Soil Mechanics, Chinese Academy of Sciences, Wuhan, Hubei 430071, China. E-mail: ttma@whrsm.ac.cn

[2]Professor, State Key Laboratory of Geomechanics and Geotechnical Engineering, Institute of Rock and Soil Mechanics, Chinese Academy of Sciences, Wuhan, Hubei 430071, China; College of Civil and Architectural Engineering, Guilin Univ. of Technology, Guilin, Guangxi 541004, China (corresponding author). E-mail: cfwei@whrsm.ac.cn

[3]Graduate Student, State Key Laboratory of Geomechanics and Geotechnical Engineering, Institute of Rock and Soil Mechanics, Chinese Academy of Sciences, Wuhan, Hubei 430071, China. E-mail: xxllike@126.com

[4]State Key Laboratory of Geomechanics and Geotechnical Engineering, Institute of Rock and Soil Mechanics, Chinese Academy of Sciences, Wuhan, Hubei 430071, China. E-mail: jiazuoz@gmail.com

[5]State Key Laboratory of Geomechanics and Geotechnical Engineering, Institute of Rock and Soil Mechanics, Chinese Academy of Sciences, Wuhan, Hubei 430071, China. E-mail: pchen@whrsm.ac.cn

Note. This manuscript was submitted on June 11, 2015; approved on October 12, 2015; published online on December 29, 2015. Discussion period open until May 29, 2016; separate discussions must be submitted for individual papers. This paper is part of the ***Journal of Performance of Constructed Facilities***, © ASCE, ISSN 0887-3828.

can be determined rapidly, especially when the pore water has a low potential or the soil saturation is low (Spaans and Baker 1996). Perhaps because of this, the SFCC as determined is commonly used to rapidly infer the SWCC (Spaans and Baker 1996; Bittelli et al. 2003; Flerchinger et al. 2004, 2006). In sharp contrast, the SWCC determination is generally time-consuming and becomes increasingly inaccurate when equilibration time is long as the soil sample dries.

Although the freezing point depression method sometimes yields good results in determining the SWCC for the soil water potential down to −10 MPa (Suzuki 2004; Bittelli et al. 2003), application of this procedure must be exercised with caution. Black and Tice (1989) determined the soil water characteristic curve using the modified Clapeyron equation and the measured soil freezing characteristic curve, and found that reliable results could only be obtained with suitable adjustment to the surface tension. In addition, there were few experimental results about the comparison between SWCC and SFCC when the soil water potential was less than −10 MPa. Recently, Wen et al. (2012) used an innovative sensor to directly measure the soil matric potential in the subfreezing environment and found that the matric potentials in the frozen soils were significantly higher (less negative) than the theoretical values inferred from the freezing point depression. These authors attributed the discrepancy to the adsorptive and osmotic effects.

In this study, the pulsed NMR technique was used to measure the liquid water content in frozen soils at different temperatures to determine the soil freezing characteristic with a temperature down to −39°C. The applicability and capability of this technique was clearly demonstrated by many experimental studies (Black and Tice 1989; Ishizaki et al. 1996; Smith and Tice 1988; Tice et al. 1983; Tian et al. 2014). The soil moisture characteristic curves with the largest negative water potential, approximately 300 MPa, were obtained by pressure plate and vapor equilibrium method. The relation between the two characteristic curves was investigated based on the experimental results. The effect of solutes on the pore water potential was also investigated.

## Theoretical Background

Consider a representative volume of the frozen soil of concern. Supposed that the frozen soil is in thermodynamic equilibrium, and thus the chemical potentials of each species between two different bulk phases is the same. In particular, for the solvent ($H_2O$) species in the frozen soil, $\mu^{l_{H_2O}} = \mu^{i_{H_2O}}$, in which $\mu^{l_{H_2O}}$ and $\mu^{i_{H_2O}}$ are the chemical potentials of species $H_2O$ in the unfrozen pore water and the pore ice, respectively. According to Wei (2014), one has

$$\mu^{l_{H_2O}}(T, p^l) = \tilde{\mu}_{\oplus}^{l_{H_2O}}(T, p_{atm}) + \frac{p^l}{\rho_{\oplus}^{l_{H_2O}}} + \frac{RT}{M_{H_2O}} \ln a^{l_{H_2O}} + \Omega^l.$$

in which $\tilde{\mu}_{\oplus}^{l_{H_2O}}$ is the chemical potential of pure water at temperature $T$ and the atmospheric pressure $p_{atm}$, and $\tilde{\mu}_{\oplus}^{l_{H_2O}}(T, p_{atm}) = \tilde{\mu}_0^{l_{H_2O}}(T_0, p_{atm}) - \int_{T_0}^{T}(h_l/T)dT$, in which $h_l$ is the enthalpy per mole of water; $p^l$ is the *true* pore water pressure; $\rho_{\oplus}^{l_{H_2O}}$ is the mass density of pure water, which is assumed to be constant; $T_0$ is the temperature at the reference state; $R$ is the universal gas constant; $M_{H_2O}$ is the molar mass of water; $a^{l_{H_2O}}$ is the activity of water that is a function of $T$, $p^l$, and solute concentration; $\Omega^l$ is the surface energy potential accounting for the physic-chemical interactions between the soil matrix and the pore water. Because of the physicochemical origin of $\Omega^l$, Eq. (1) clearly accounts for the effects of osmosis, sorption, and capillarity.

Assuming that the pore ice contains species $H_2O$ only, the chemical potential of ice can be expressed as

$$\mu^{i_{H_2O}} = \tilde{\mu}_{\oplus}^{i_{H_2O}}(T, p_{atm}) + \frac{p^i}{\rho_{\oplus}^{i_{H_2O}}} \tag{2}$$

in which $\tilde{\mu}_{\oplus}^{i_{H_2O}}$ = chemical potential of the pure ice at $T$ and $p_{atm}$; $p^i$ = pore ice pressure; $\rho_{\oplus}^{i_{H_2O}}$ = mass density of the pure ice. Here the pore ice in the frozen soils can be assumed as the non-wetting phase, on which the effect of capillary and adsorption can be neglected. At the reference state, if the freezing point of the pure water is $T_0$

$$\tilde{\mu}_{\oplus}^{i_{H_2O}}(T, p_{atm}) = \tilde{\mu}_0^{i_{H_2O}}(T_0, p_{atm}) - \int_{T_0}^{T} \frac{h_i}{T} dT \tag{3}$$

in which $h_i$ = enthalpy per mole of ice.

In the frozen soils, the unfrozen pore water and pore ice can coexist in equilibrium under temperatures well below the normal freezing point (Flerchinger et al. 2006), and under such a condition, $\mu^{l_{H_2O}} = \mu^{i_{H_2O}}$. Using Eqs. (1)–(3), and noting that $\tilde{\mu}_0^{l_{H_2O}} = \tilde{\mu}_0^{i_{H_2O}}$, one can derive

$$L_f \ln\left(\frac{T_0 - T}{T_0}\right) = \frac{p^l}{\rho_{\oplus}^{l_{H_2O}}} + \frac{RT}{M_{H_2O}} \ln a^{l_{H_2O}} + \Omega^l - \frac{p^i}{\rho_{\oplus}^{i_{H_2O}}} \tag{4}$$

in which $L_f$ $(=h_l - h_i)$ is the latent heat of fusion, which is assumed to be independent of the temperature. Eq. (4) is a generalized Clapeyron equation, which describes the criterion for the phase transition between liquid water and ice in the soil pores.

Similarly, in the unsaturated soils, the chemical potential of $H_2O$ in the pore air can be expressed as

$$\mu^{g_{H_2O}} = \tilde{\mu}_{\oplus}^{g_{H_2O}}(T, p_{atm}) + \frac{RT}{M_{H_2O}} \ln \frac{p^{g_{H_2O}}}{p_{atm}} \tag{5}$$

in which $\tilde{\mu}_{\oplus}^{g_{H_2O}}$ = chemical potential of the fully saturated $H_2O$ vapor at $T$ and $p_{atm}$, at which $\tilde{\mu}_{\oplus}^{g_{H_2O}} = \tilde{\mu}_{\oplus}^{l_{H_2O}}$; $p^{g_{H_2O}}$ = partial pressure of $H_2O$ in the pore air.

In applying the vapor equilibrium technique, $\mu^{l_{H_2O}} = \mu^{g_{H_2O}}$, one can derive

$$\frac{RT}{M_{H_2O}} \ln H_r = \frac{p^l}{\rho_{\oplus}^{l_{H_2O}}} + \frac{RT}{M_{H_2O}} \ln a^{l_{H_2O}} + \Omega^l \tag{6}$$

in which $H_r$ $(=p^{g_{H_2O}}/p_{atm})$ = relative humidity of the air in a closed chamber containing the soil sample and a solution reservoir.

We have supposed that all the measurements are performed under an ambient pressure of $p_{atm}$. Under such a circumstance, the ice pressure in the frozen soil experiment is practically equal to the atmospheric pressure, and the term $p^i/\rho_{\oplus}^{i_{H_2O}}$ can be dropped from Eq. (4), so that the right-hand sides of both Eqs. (4) and (6) are *formally* the same. In the terminology of soil science, the right side of Eq. (4) simply equals the total potential of soil water, $\psi$. In general, $\psi$ depends upon the ambient temperature and the pore water concentration as well as the soil properties, including porosity, composition, surface characteristics, fixed-charge density, and so on. Eqs. (4) and (6) imply that the total soil water potential, $\psi$, can be measured by either the vapor equilibrium technique or the freezing point depression method. Remarkably, however, the $\psi$ values measured by these two methods are generally not equal to each other even at the same (unfrozen) water saturation.

To explore further the character of the total water potential, we now consider a system consisting of a representative volume of the unsaturated soil under consideration and a reservoir containing a

water solution with the same compositions as the pore water. We have supposed that the solution in the reservoir is connected to the pore water in the soil through a tube, and the whole system is in thermodynamic equilibrium under temperature of $T$ and an ambient pressure of $p_{\text{atm}}$. For convenience, the water solution in the reservoir is called the "equilibrium solution" hereinafter. The pressure of the equilibrium solution is $p_W^l$, while the activity of its solvent is $a_W^{l_{H_2O}}$. According to Wei (2014), the total water potential can be rewritten as

$$\psi = \frac{p_W^l}{\rho_{\oplus}^{l_{H_2O}}} + \frac{RT}{M_{H_2O}} \ln a_W^{l_{H_2O}} \tag{7}$$

in which $p_W^l = p^l - \Pi$, and $\Pi$ is the generalized osmotic pressure, given by

$$\Pi = -\frac{RT\rho_{\oplus}^{l_{H_2O}}}{M_{H_2O}} \ln\left(\frac{a^{l_{H_2O}}}{a_W^{l_{H_2O}}}\right) - \rho_{\oplus}^{l_{H_2O}} \Omega^l \tag{8}$$

In the terminology of soil science, the first term in the right-hand side of Eq. (7) is simply equal to the matric potential (denoted by $\psi_m$), while the second term is the osmosis potential (denoted by $\psi_o$). From Eq. (7), it is clear that $\psi$ is generally temperature-dependent, because both $p_W^l$ and $a_W^{l_{H_2O}}$ are influenced by the temperature. Indeed, $\psi$ is very sensitive to the temperature, as shown by the generalized Clapeyron equation [i.e., Eq. (4)]. For example, a 0.01°C error in the temperature measurement can cause an error of several kilopascals in determining $\psi$. Therefore, the accuracy of the temperature sensor can significantly influence the "measured" value of $\psi$.

## Experimental Program

### Soil Properties and Sample Preparation

Silty and clayey soils were used in the experiment. The selected physical properties of the tested soils are presented in Table 1. The soils were air-dried first and then carefully wetted to a prescribed water content using deionized water, which is equivalent to a specified water content of 16% for silt or 20% for clay. Then the soils were put in tightly covered plastic bags and stored in a container with both temperature and humidity being controlled for 2 days for moisture equilibration. All the samples were statically compacted in a Teflon cylinder with a cross-sectional area of 16 $cm^2$ and a height of 2 cm to the targeted dry densities (1.6 $g/cm^3$ for silt and 1.4 $g/cm^3$ for clay).

### Determination of Soil Water Characteristic Curves

Typical techniques for measuring the SWCC include the tensiometer, the axis-translation technique, and the vapor equilibrium technique. For a detailed analysis of their advantages and limitations, interested readers can refer to related references (e.g., Ridley and Wray 1996; Lu and Likos 2004). In this study, the pressure plate extractor and vapor equilibrium technique were used to determine the SWCCs at high and low water content, respectively. The measured SWCCs of the silt and the clay are shown in Figs. 1 and 2, respectively.

In Fig. 1, the wetting curve of silt was obtained by 1-D pressure plate contractor. It is clear that the SWCCs show clear hysteresis during a wetting-drying cycle. When the sample was wetted to $s_c = 0$ kPa, the degree of saturation was about 84% and a certain amount of air was trapped in the pores. Clearly, the data points for drying obtained by both the vapor equilibrium technique and the pressure plate method are roughly located on a smooth curve.

A similar trend can be observed in Fig. 2, where the measured drying SWCC for the clay is presented. Noticeably, however, the data points determined by the pressure plate method under the water content less than 0.17 deviate significantly from the overall trend of the drying curve. The discrepancy can be attributed to the possible disequilibrium of the system during the measurement (Madsen et al. 1986; Campbell 1988). As water content (or saturation) decreases, the water phase in the pores tends to be discontinuous. Hence, at low saturation, if the pressure plate method is applied, it is difficult for the soil water to become equilibrated, so that significant error could exist in the water content measurement (Campbell 1988). Indeed, it has been well recognized that, at low saturation, the water potential determined by pressure plate was

**Table 1.** Physical Properties of the Tested Soils

| Soil | Specific surface area ($m^2/g$)[a] | Specific gravity | Liquid limit | Plastic limit | Particle size distribution (%) 0.25–0.075 | 0.075–0.005 | <0.005 |
|---|---|---|---|---|---|---|---|
| Silt | 6.22 | 2.68 | 29.4 | 19.8 | 17.7 | 79.4 | 2.9 |
| Clay | 22.63 | 2.71 | 27.6 | 15.6 | 0 | 80.3 | 19.7 |

[a]via BET method by adsorption of $N_2$ on desorption process.

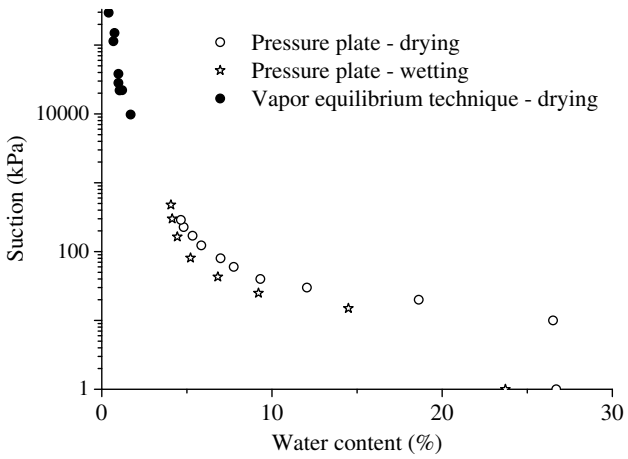


**Fig. 1.** Measured SWCCs of silt

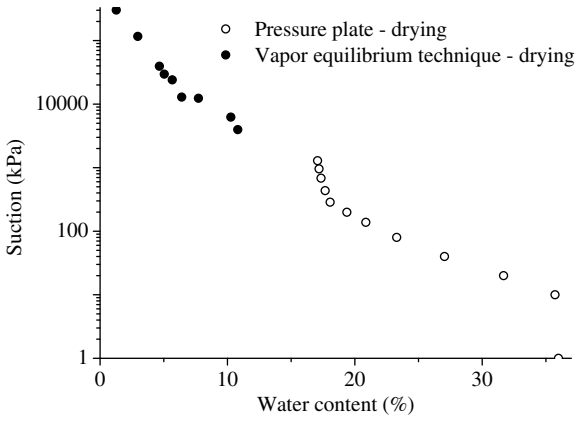


**Fig. 2.** Measured SWCCs of clay

always lower than that by other methods, such as thermocouple psychrometer (Madsen et al. 1986) and osmotic tensiometer (Peck and Rabbidge 1969).

### *Determination of Soil Freezing Characteristic Curve*

A temperature-control bath was used to control the freezing temperature. To prevent the effect of supercooling, the temperature was slowly increased step by step from −40 to 20°C. When the sample reached thermal equilibrium (usually, it took 4 to 10 h) under the controlled temperature, the sample was moved to the low-field nuclear magnetic resonance (NMR) system to measure the unfrozen water content, where the sample was isolated from the environment. During the NMR measurements, the temperature of the NMR sample tube was controlled to approximately equal the temperature of the frozen sample to prevent the pore ice from melting. The temperature-controlling unit has an accuracy of 0.1°C. To calibrate the temperature, one sensor with the precision of 0.01°C was inserted into the soil sample to measure the temperature accurately.

#### Distribution of Unfrozen Water

Figs. 3 and 4 depict the distribution curves of the NMR relaxation time $T_2$ for silt and clay at different temperatures during the thawing process. Low-field nuclear magnetic resonance (NMR) can be used to explore the water distribution in soils via detecting the signal of hydrogen atoms in $H_2O$ (Tian et al. 2014). The horizontal axis $T_2$ is the proton spin-spin relaxation time, which is linearly proportional to the characteristic size of the pores saturated with water. The vertical axis cumulative signals represent the water content at the corresponding pore ($T_2$ value). Hence, according to the $T_2$ distribution, one can obtain the variation of pore water content and its distribution in the soils (Tian et al. 2014).

In these two figures, the NMR signal intensity in the range of larger $T_2$ increases with the increase of temperature, which indicates that the water in small pores thaws first and then continues in larger pores as temperature increases. This phenomenon is analogous to soil wetting, which can be explained by referring to the energy status of the pore water (Tian et al. 2014). Indeed, compared to the free pore water or the pore water in larger pores, the bound water and the water in smaller pores has lower activity due to stronger capillary and adsorptive effects. Hence, both drying and freezing are prone to occur in larger pores, whereas wetting and thawing take place in smaller pores first. With the further decrease of the soil water potential (lower temperature), the water content changes more slowly. Unfrozen water can exist in the soil mainly as the form of the absorbed electric double layer water or adsorbed water. Clearly, the NMR test result is consistent with the analysis stated above. The microscopic properties, which can be detected by NMR technique, provide instructive information to interpret the soil behavior.

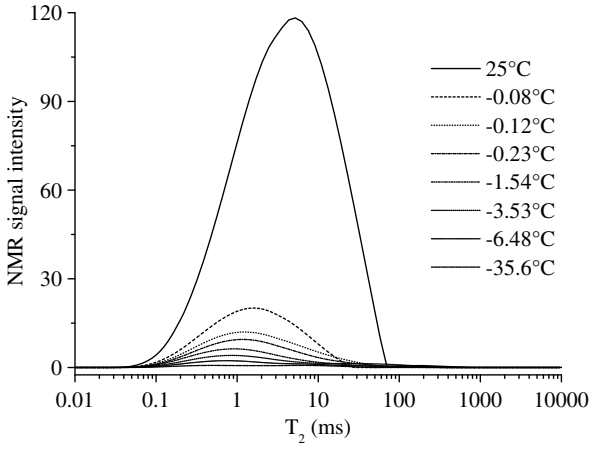


**Fig. 3.** T2 distribution curves of the silt sample during the thawing process

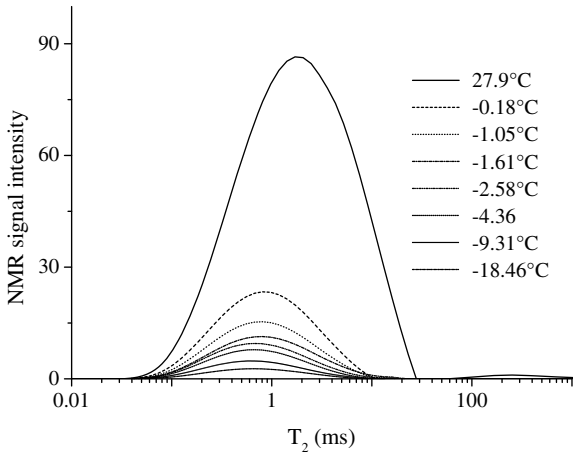


**Fig. 4.** T2 distribution curves of the clay sample during the thawing process

#### Unfrozen Water Content

The area under the $T_2$ distribution curve represents the population of water molecules and serves as an indicator of the amount of unfrozen water in the soil sample (Black and Tice 1989; Ishizaki et al. 1996; Smith and Tice 1988; Tice et al. 1983). When the sample remains unfrozen (the temperature is greater than zero), the NMR signal peak area increases with the decrease of temperature, which should be corrected according to the Curie law (Tice et al. 1983). There is a linear relationship between the NMR signal peak area and temperature at the fully saturated state. Based on the method of Tice et al. (1983), the temperature-correction on the NMR signal can be made by linearly extrapolating the NMR signal peak area of the total pore water in the soil under the unfrozen condition to the frozen condition. The fraction of unfrozen pore water at various temperatures can be calculated by the ratio of the measured NMR signal peak area to the corrected value by linearly extrapolating at the corresponding temperature. Fig. 5 illustrates the variations of unfrozen water content with temperature for silt

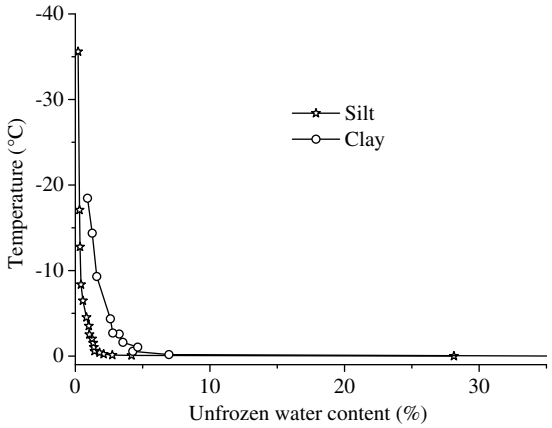


**Fig. 5.** Soil freezing characteristic curves

and clay. As the temperature dropped below 0°C, the amount of unfrozen water decreased, initially in a drastic way and then gradually. At the same temperature, the unfrozen water content of clay is higher than that of silt, due to the stronger water retaining capacity.

As temperature decreases, most water freezes, and the remaining unfrozen water exists in progressively thinner adsorbed films and smaller pores and crevices. When the temperature drops down to −39°C, there still exists a thin water film coating on the particles. The unfrozen water film can provide the passage for the unfrozen pore water to move toward the ice lens, resulting in the growth of ice lens and finally the occurrence of the frost heave (Wettlaufer and Worster 2006).

### Relation between SWCC and SFCC at Lower Water Content

The total soil water potential can be calculated from Eq. (4) based on the freezing point of the soil water, namely, $\psi = L_f \ln[(T_0 - T)/T_0]$, in which $L_f = 3.35 \times 10^5$ J/kg, and the unfrozen water content can be determined using the NMR measurement as stated above. The experimental results are shown in Figs. 6 and 7 (denoted by solid asterisks), where the SWCCs from the pressure plate and vapor equilibrium method are also given. It must be pointed out that, in Figs. 6 and 7, the soil water characteristic curve represents the water retention properties at room temperature (about 27°C), while the freezing characteristic curve represents the water retention properties at 0°C.

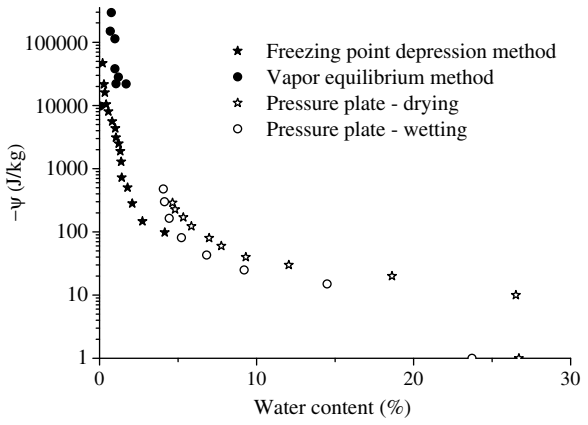


**Fig. 6.** Relationship between the water content and soil water potential for silt

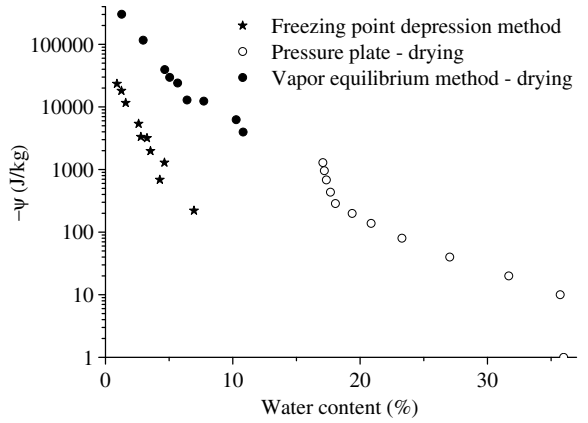


**Fig. 7.** Relationship between the water content and soil water potential for clay

Because it is generally difficult to control the temperature in the vicinity of 0°C, the SFCC cannot be accurately measured at higher temperature. Thus, only the SFCCs at lower temperature are given in Figs. 6 and 7. It can be seen that at the same water content, the soil water potential of unsaturated soils is much more negative than that of frozen soils. Koopmans and Miller (1966) introduced a soil-dependent constant to link the SFCC and SWCC, which was supposed to account for the surface energy difference between the ice-water (at 0°C) and air-water interface (at 23°C), and equal $\gamma_{aw}/\gamma_{iw}$, in which $\gamma_{aw}$ and $\gamma_{iw}$ are the excess surface energies on the air-water (at 23°C) and ice-water (at 0°C) interfaces, respectively,. These authors believed that the value of $\gamma_{aw}/\gamma_{iw}$ was approximately 2.2 at the temperatures as low as −0.15°C. They suggested that the capillary effect was dominated in the frozen sample at the temperature higher than −0.15°C, whereas the adsorptive effect was becoming increasingly important as temperature increased.

According to Spaans and Baker (1996), when the water was tightly held onto the grain surfaces by adsorptive forces, it should be considered immaterial whether pore ice or pore air is present on the other side of the unfrozen water film. That is, the reduction of the soil water potential due to adsorptive forces is identical in both cases, in which the temperatures are different. In Spaans and Baker's (1996) experiments, the SWCCs were determined by using the Temp cell and pressure chamber, and the measured matric potentials ranged from 0 to 1,500 kPa. These authors believed that the differences in the water potentials obtained from SFCC and SWCC were due to the osmotic potential only. Noticeably, the lowest temperature in these experiments was only −8°C.

In our SWCCs experiments, the matric potentials were obtained by a pressure plate extractor, and the total potentials were obtained by vapor equilibrium method. Figs. 6 and 7 show that at low water content, the total water potential obtained by the vapor equilibrium method is significantly lower than that by the freezing point depression method. Clearly, our experimental results are inconsistent with the previous results mentioned above (Koopmans and Miller 1966; Spaans and Baker 1996). To explain this discrepancy, one can refer to Eq. (7). At low water content, the matric potential ($\psi_m = p_W^l / \rho_{\oplus}^{l_{H_2O}}$) is dominated by the adsorption effect, and thus when the temperature decreases, $\psi_m$ increases (becomes less negative). In contrast, at low water content, the osmotic potential ($\psi_o = RT \ln a_W^{l_{H_2O}} / m_{H_2O}$) remains practically unchanged, and its magnitude is much smaller than that of $\psi_m$. Therefore, as the temperature decreases, the increase of the matric potential can overshadow the variation of the osmotic potential, resulting in the discrepancy observed in Figs. 6 and 7. Noticeably, the discrepancy is more pronounced in clay than in silt.

The above experimental results can be used to illustrate the shortcomings associated with the use of the SWCC to estimate the hydraulic conductivity function of partially frozen soils (Azmatch et al. 2012). Jame and Norum (1980) and Lundin (1990) mentioned that the application of the hydraulic conductivity function for unfrozen soil to frozen soil would overestimate the frost induced water fluxes, and they therefore introduced an impedance parameter to reduce the hydraulic conductivity for frozen soil (Zhao et al. 1997; Stähli et al. 1999; Hansson et al. 2004). From the above experimental results, it can be seen that, at the same water potential, the water content of an unsaturated soil is significantly greater than that of its frozen counterpart, resulting in an overestimation of the hydraulic conductivity of the frozen soil.

### Influence of Solutes

In the above discussions, we suggest that at low water content the adsorptive forces in the soils become dominant so that the matric

potential is dominated by the adsorptive part, whereas the capillary part is negligible. To examine this assumption, a series of experiments were performed to determine the SWCCs for the clayey soil at different solute concentrations. The tested materials were saturated with NaCl solutions of concentrations varying between 0 and 1.0 mol/L. Fig. 8 shows the soil water characteristic curves at different concentrations obtained by the pressure plate and vapor equilibrium methods. The pressure plate was used to measure the matric potential component of pore water potential, while the vapor equilibrium method was used to measure the total water potential. Fig. 8 shows that the solute concentration has a relatively slight effect on the matric potential (measured via the pressure plate method), though it can significantly influence the total potential (measured via the vapor equilibrium technique). In the vapor equilibrium experiments, as the water content decreases, the fraction of osmotic potential in the total potential decreases, due to the increase of matric potential (through the increase of the adsorptive component). Fig. 9 depicts the freezing characteristic curves at different concentrations using the freezing depression method. It is clear that the unfrozen water content at the same temperature increases with the increase of solute concentration. The clay samples, saturated by the NaCl solution, remained unfrozen at a temperature of a few degrees lower than 0°C. This is because the existence of solutes and the effect of capillarity can depress the freezing point temperature.

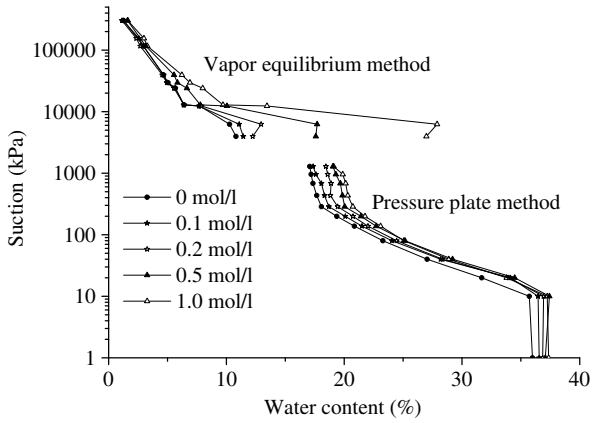


**Fig. 8.** Measured SWCCs of clay at different NaCl concentrations

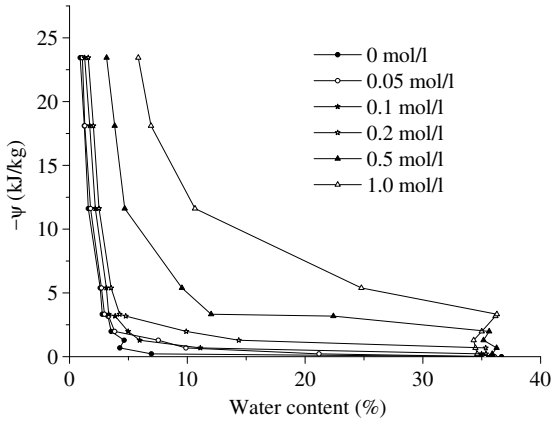


**Fig. 9.** Relationship between unfrozen water content and soil water potential of clay at different NaCl concentrations

## Results and Discussions

At low water saturation, the liquid (unfrozen) water exists in the pores primarily as the water films coating the soil grain surfaces, and free water can only exist in the crevices between soil grains. Under this condition, adsorptive surface forces begin to dominate over capillary forces. The adsorptive forces stem from the physicochemical interactions between the soil particles and the water films (Nitao and Bear 1996), including electrostatic force between the electric charges on the particles and the water molecules, van der Waals force, and hydration force due to the polarity of water molecule. In general, the thickness of the water films is in the range of 1–100 nm, much smaller than the pore size.

In general, the equilibrium solution pressure, $p_W^l$, in Eq. (7) has several contributions, which stem from the ambient air pressure, gravity, capillarity, and adsorption, respectively. Note that the ambient air pressure equals the atmospheric pressure in all the experiments. At low water saturation, the effects of gravity and capillarity are negligible, and thus $p_W^l$ can be considered as approximately the negative of the adsorptive forces (collectively denoted as $\Phi$), i.e., $p_W^l \sim -\Phi$. According to Israelachvili (2011), $\Phi$ can be divided into nonpolar van der Waals force and polar interactions, and if the electrostatic effect is neglected, one can write

$$\Phi = -\frac{A_H}{6\pi h^3} + \frac{V_{HR}^0}{h_0}\exp\left(-\frac{h}{h_0}\right) \tag{9}$$

The first term at the right hand of Eq. (9) denotes the van der Waals force of particles; $h$ is the average thickness of the water films; $A_H$ is the Hamaker constant for the solid-vapor interactions through the intervening liquid, and related to the dielectric constant. The range of $A_H$ is approximately $-10^{-19}$ to $-10^{-20}$ J for soils, in which $-6 \times 10^{-20}$ J is an effective value (Tuller and Or 2005). The second term of the right hand of Eq. (9) is hydration force, which is attributed to the changes in the structure of water adjacent to solid surfaces and deformation of hydrated shells (Paunov et al. 1996). $V_{HR}^0$ is the polar components of spreading coefficient, and $h_0$ is a correlation length for the polar fluid. For water, $h_0$ appears to be in the range of 0.2 to 1 nm. When the thickness of water film decreases to 10 nm, the structural force begins to be active and increases rapidly with the decrease of the film thickness.

The thickness of the water film can be expressed as a function of soil specific surface area and gravimetric water content (Tuller and Or 2005), i.e.

$$h = \frac{w}{S_a \rho_w} \tag{10}$$

in which $S_a$ = soil specific surface area ($m^2/g$). As a first approximation, it is assumed that water in the vicinity of the surface has the same density, $\rho_w$, as bulk water. From Eqs. (9) and (10), the relationship between the gravimetric water content and adsorptive force can be developed, which can be expressed as $w = f(\Pi)$.

At lower water content, $\Psi$ and $\Phi$ can be calculated using Eqs. (7), (9), and (10), provided that the salinity of the equilibrium solution and the gravimetric water content of the soil are given. The calculated results are presented in Figs. 10–12. In calculation, it is assumed that the pore water is a dilute solution so that $a_W^{l_{H_2O}} \approx x^{l_{H_2O}}$, in which $x^{l_{H_2O}}$ is the molar fraction of solvent in the equilibrium solution; the material parameters assume the following values: $A_H = -6 \times 10^{-20}$ J and $h_0 = 0.8$ nm for both SFCC and SWCC, while $V_{HR}^0 = 0.32$ N/m for SWCC and $V_{HR}^0 = 0.008$ N/m for SFCC. In addition, it is assumed that the soil-water interaction depends practically upon the thickness of the adsorbed

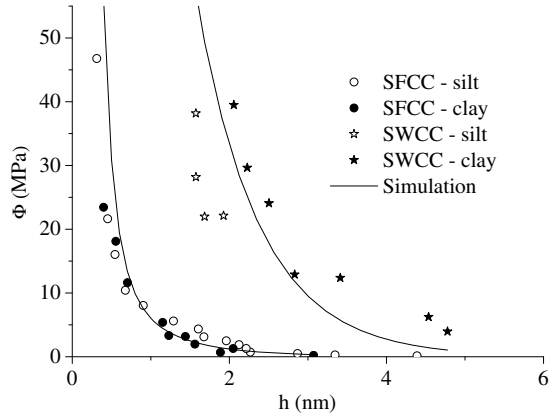


**Fig. 10.** Relationship between the intermolecular force and the water film thickness

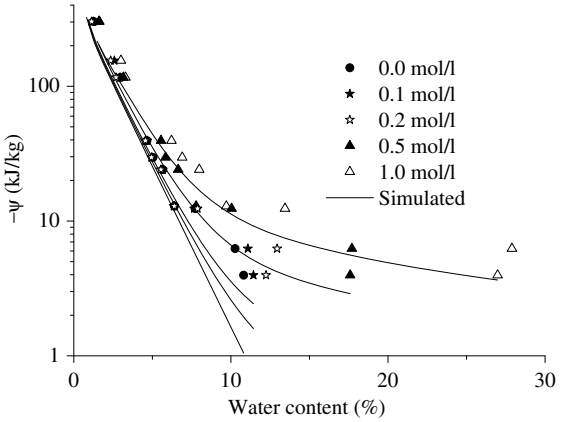


**Fig. 11.** Comparison of the measured and simulated relationships between water content and water potential of clay at lower water saturation (from SWCCs)

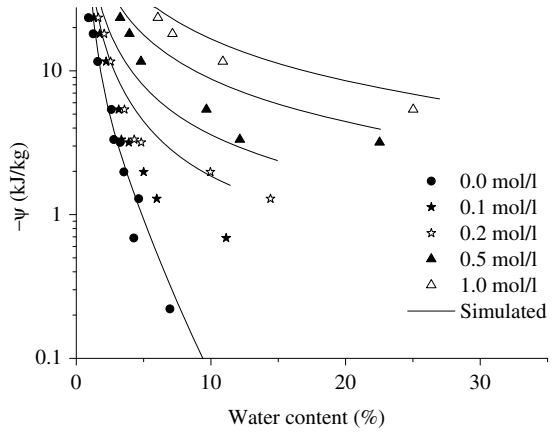


**Fig. 12.** Comparison of the measured and simulated relationships between water content and water potential of clay at lower water saturation (from SFCCs)

water film only and independent of the character of the grain surfaces. This, of course, is not true in the real situation. However, because the effect of the surface characters can somewhat be represented by the water film thickness, the above assumption is adopted here. Such an assumption was also adopted in some previous works (e.g., Low 1994).

The calculated results of Eq. (9) for the two soils saturated with deionized water are depicted in Fig. 10, where the results calculated from the SWCCs and SFCCs are also given for comparison. It can be seen that the simulations of Eq. (9) agree reasonably well with the results calculated from the SWCCs and SFCCs.

The effects of salinity and water content on Ψ and Φ are shown in the Figs. 11 and 12 for the clayey soil. Here, the solute is assumed as non-volatile and the ice does not contain solutes (Hobbs 1974). As the amount of water decreases, pore water concentration increases and the solution becomes denser and denser. It is clear that the calculated total water potentials agree reasonably well with the measurements, implying that Eq. (9) and its related assumptions are reasonable. The discrepancy can be attributed to the following reasons: (1) the solution is not ideal; (2) there exists some coupling between the matric potential and osmotic potential; and (3) the ice contains some solutes, so that the potential component contributed by osmosis decreases.

## Conclusions

The relation between SFCCs of frozen soils and SWCCs of unsaturated soils is investigated based on the similarity between the freezing/thawing and the drying/wetting processes in soils. It is experimentally shown that the total water potential of an unsaturated soil is more negative than that of its frozen counterpart at the same water content. Two competitive mechanisms are invoked to explain this phenomenon, i.e., the matric potential increases as temperature decreases, whereas the osmotic potential decreases. At low water saturation, the osmotic pressure becomes dominant in the total water potential, resulting in the phenomenon observed in the above experiments.

The water retention properties of soils are also investigated based on the measurements of the SWCCs and SFCCs of a clay saturated with NaCl solutions at various concentrations. Based on the principles of the surface chemistry, a relationship between the water content and intermolecular force at the dry end is developed. It is shown that under the adsorption condition the so-called suction can increase almost infinitely due to the effect of intermolecular forces. The results from this study indicate that the freezing point depression method should be used with caution to determine the soil water retention curve at lower water saturation.

## Acknowledgments

The research was supported by the Natural Science Foundation of China under Grant No. 11502276 and 41572293, and the Natural Science Foundation of Guangxi under Grant No. 2012GXNSFGA060001.

## References

Azmatch, T. F., Sego, D. C., Arenson, L. U., and Biggar, K. W. (2012). "Using soil freezing characteristic curve to estimate the hydraulic conductivity function of partially frozen soils." *Cold Reg. Sci. Technol.*, 83–84, 103–109.

Bachmann, J., and van der Ploeg, R. R. (2002). "A review on recent developments in soil water retention theory: Interfacial tension and temperature effects." *J. Plant Nutr. Soil Sci.*, 165(4), 468–478.

Bittelli, M., Flury, M., and Campbell, G. S. (2003). "A thermodielectric analyzer to measure the freezing and moisture characteristic of porous media." *Water Resour. Res.*, 39(2), 1041.

Black, P. B., and Tice, A. R. (1989). "Comparison of soil freezing curve and soil water curve data for Windsor sandy loam." *Water Resour. Res.*, 25(10), 2205–2210.
Campbell, G. S. (1988). "Soil water potential measurement: An overview." *Irrig. Sci.*, 9(4), 265–273.
Cannel, G. H., and Gardner, W. H. (1959). "Freezing-point depressions in stabilized aggregates, synthetic soil, and quartz sand." *Soil Sci. Soc. Am. Proc.*, 23(6), 418–422.
Dash, J. G., Fu, H., and Wettlaufer, J. S. (1995). "The premelting of ice and its environmental consequences." *Rep. Prog. Phys.*, 58(1), 115–167.
Drotz, H. H., Tilston, E. L., Sparrman, T., Schleucher, J., Nilsson, M., and Öquist, M. G. (2009). "Contributions of matric and osmotic potentials to the unfrozen water content of frozen soils." *Geoderma*, 148(3–4), 392–398.
Flerchinger, G. N., Seyfried, M. S., and Hardegree, S. P. (2004). "Estimation of the soil moisture characteristic curve from the soil freezing characteristic." *ASAE/CSAE Annual Int. Meeting*, Washington, DC, 1–13.
Flerchinger, G. N., Seyfried, M. S., and Hardegree, S. P. (2006). "Using soil freezing characteristics to model multi-season soil water dynamics." *Vadose Zone J.*, 5(4), 1143–1153.
Hansson, K., Simunek, J., Mizoguchi, M., Lundin, L. C., and van Genuchten, M. (2004). "Water flow and heat transport in frozen soil: Numerical solution and freeze-thaw applications." *Vadose Zone J.*, 3(2), 693–704.
Hobbs, P. V. (1974). *Ice physics*, Clarendon Press, Oxford, U.K.
Ishizaki, T., Maruyama, M., Furukawa, Y., and Dash, J. G. (1996). "Premelting of ice in porous silica glass." *J. Cryst. Growth*, 163(4), 455–460.
Israelachvili, J. N. (2011). *Intermolecular and surface forces*, 3rd Ed., Academic Press, Burlington.
Jame, Y. W., and Norum, D. I. (1980). "Heat and mass transfer in freezing unsaturated porous media." *Water Resour. Res.*, 16(4), 811–819.
Koopmans, R. W. R., and Miller, R. D. (1966). "Soil freezing and soil water characteristic curves." *Soil Sci. Soc. Am. Proc.*, 30(6), 680–685.
Low, P. F. (1994). "The clay/water interface and its role in the environment." *Prog. Colloid Polym. Sci.*, 95, 98–107.
Lu, N., and Likos, W. J. (2004). *Unsaturated soil mechanics*, Wiley, New York.
Lundin, L. C. (1990). "Hydraulic properties in an operational model of frozen soil." *J. Hydrol.*, 118(1–4), 289–310.
Madsen, H. B., Jensen, C. R., and Boysen, T. (1986). "A comparison of the thermocouple psychrometers and the pressure plate methods for determination of soil water characteristic curves." *J. Soil Sci.*, 37(3), 357–362.
Miller, R. D. (1966). "Phase equilibria and soil freezing." *Proc., 2nd Int. Conf. in Permafrost*, National Academy of Sciences, National Research Council, Washington, DC, 193–197.
Miller, R. D. (1980). "Freezing phenomena in soils." *Applications of soil physics*, D. Hillel, ed., Academic Press, New York, 254–299.
Nitao, J. J., and Bear, J. (1996). "Potentials and their role in transport in porous media." *Water Resour. Res.*, 32(2), 225–250.
Paunov, V. N., Dimova, R. I., Kralchevsky, P. A., Broze, G., and Mehreteab, A. (1996). "The hydration repulsion between charged surfaces as an interplay of volume exclusion and dielectric saturation effects." *J. Colloid Interface Sci.*, 182(1), 239–248.
Peck, A. J., and Rabbidge, R. M. (1969). "Design and performance of an osmotic tensiometer for measuring capillary potential." *Soil Sci. Soc. Am. Proc.*, 33(2), 196–202.
Ridley, A. M., and Wray, W. K. (1996). "Suction measurement: A review of current theory and practices—State of the art report." *Proc., 1st Int. Conf. on Unsaturated Soils*, Balkema, Rotterdam, Netherlands, 1293–1322.
Smith, M. W., and Tice, A. R. (1988). "Measurement of the unfrozen water content of soils: Comparison of NMR and TDR method." *CRREL Rep.*, U.S. Cold Regions Research and Engineering Laboratory, Hanover, NH, 88–18 .
Spaans, E. J. A., and Baker, J. M. (1996). "The soil freezing characteristic: Its measurement and similarity to the soil moisture characteristic." *Soil Sci. Soc. Am. J.*, 60(1), 13–19.
Stähli, M., Jansson, P. E., and Lundin, L. C. (1999). "Soil moisture redistribution and infiltration in frozen sandy soils." *Water Resour. Res.*, 35(1), 95–103.
Suzuki, S. (2004). "Dependence of unfrozen water content in unsaturated frozen clay soil on initial soil moisture content." *Soil Sci. Plant Nutr.*, 50(4), 603–606.
Tian, H. H., Wei, C. F., Wei, H. Z., Yan, R. T., and Chen, P. (2014). "Freezing and thawing characteristics of frozen soils: Bound water content and hysteresis phenomenon." *Cold Reg. Sci. Technol.*, 103, 74–81.
Tice, A. R., Oliphant, J. L., Zhu, Y. L., Nakano, Y., and Jenkins, T. F. (1983). "Relationship between the ice and unfrozen water phases in frozen soils as determined by pulsed nuclear resonance and physical desorption data." *J. Glaciol. Cryopedology*, 5(2), 37–46 (in Chinese).
Torrance, J. K., and Schellekens, F. J. (2006). "Chemical factors in soil freezing and frost heave." *Polar Rec.*, 42(1), 33–42.
Tuller, M., and Or, D. (2005). "Water films and scaling of soil characteristic curves at low water contents." *Water Resour. Res.*, 41(9), W09403.
Watanabe, K., and Flury, M. (2008). "Capillary bundle model of hydraulic conductivity for frozen soil." *Water Resour. Res.*, 44(12), W12402.
Watanabe, K., and Mizoguchi, M. (2002). "Amount of unfrozen water in frozen porous media saturated with solution." *Cold Reg. Sci. Technol.*, 34(2), 103–110.
Watanabe, K., and Wake, T. (2009). "Measurement of unfrozen water content and relative permittivity of frozen unsaturated soil using NMR and TDR." *Cold Reg. Sci. Technol.*, 59(1), 34–41.
Wei, C. F. (2014). "A theoretical framework for modeling the chemomechanical behavior of unsaturated soils." *Vadose Zone J.*, 13(9), 1–12.
Wen, Z., et al. (2012). "Experimental study on unfrozen water content and soil matric potential of Qinghai-Tibetan silty clay." *Environ. Earth Sci.*, 66(5), 1467–1476.
Wettlaufer, J. S., and Worster, M. G. (2006). "Premelting dynamics." *Annu. Rev. Fluid Mech.*, 38(1), 427–452.
Zhao, L., Gray, D. M., and Male, D. H. (1997). "Numerical analysis of simultaneous heat and mass transfer during infiltration into frozen ground." *J. Hydrol.*, 200(1–4), 345–363.